Title

Betacellulin drives therapy resistance in glioblastoma

Journal

Neuro-Oncology, 22(4)

ISSN

1522-8517

Authors

Fan, Qiwen
An, Zhenyi
Wong, Robyn A
et al.

Publication Date

2020-04-15

DOI

10.1093/neuonc/noz206

Peer reviewed

Neuro-Oncology
22(4), 457–469, 2020 | doi:10.1093/neuonc/noz206 | Advance Access date 3 November 2019

Betacellulin drives therapy resistance in glioblastoma

QiWen Fan,[†] Zhenyi An,[†] Robyn A. Wong, Xujun Luo, Edbert D. Lu, Albert Baldwin, Manasi K. Mayekar, Franziska Haderk, Kevan M. Shokat, Trever G. Bivona, and William A. Weiss

Department of Neurology, University of California San Francisco (UCSF), San Francisco, California (Q.F., Z.A., R.A.W., X.L., E.L., W.A.W.); Howard Hughes Medical Institute and Department of Cellular and Molecular Pharmacology, University of California San Francisco, San Francisco, California (K.M.S.); Helen Diller Family Comprehensive Cancer Center, San Francisco, California (Q.F., Z.A., R.A.W., X.L., E.L., M.K.M., F.H., T.G.B., W.A.W.); Department of Pediatrics, University of California San Francisco, San Francisco, California (W.A.W.); Department of Neurological Surgery, University of California San Francisco, San Francisco, California (W.A.W.); Comprehensive Cancer Center, University of North Carolina at Chapel Hill, Chapel Hill, North Carolina (A.B)

[†]These authors contributed equally to this work.

Corresponding Author: William A. Weiss, 1450 3rd St, room 277, San Francisco, CA 94158 (waweiss@gmail.com).

Abstract

Background. The transcription factor signal transducer and activator of transcription 3 (STAT3) drives progression in glioblastoma (GBM), suggesting STAT3 as a therapeutic target. Surprisingly however, GBM cells generally show primary resistance to STAT3 blockade.

Methods. Human glioblastoma cell lines LN229, U87, SF767, and U373, and patient-derived xenografts (PDXs) GBM8 and GBM43 were used to evaluate epidermal growth factor receptor (EGFR) activation during STAT3 inhibition. Protein and gene expression experiments, protein stability assays, cytokine arrays, phospho-tyrosine arrays and EGFR-ligand protein arrays were performed on STAT3 inhibitor–treated cells. To evaluate antitumor activity, we administered a betacellulin (BTC)-neutralizing antibody alone and in combination with STAT3 inhibition. BTC is an EGFR ligand. We therefore treated mice with orthotopic xenografts using the third-generation EGFR inhibitor osimertinib, with or without STAT3 knockdown.

Results. We demonstrate that both small-molecule inhibitors and knockdown of STAT3 led to expression and secretion of the EGFR ligand BTC, resulting in activation of EGFR and subsequent downstream phosphorylation of nuclear factor-kappaB (NF-κB). Neutralizing antibody against BTC abrogated activation of both EGFR and NF-κB in response to inhibition of STAT3; with combinatorial blockade of STAT3 and BTC inducing apoptosis in GBM cells. Blocking EGFR and STAT3 together inhibited tumor growth, improving survival in mice bearing orthotopic GBM PDXs in vivo.

Conclusion. These data reveal a feedback loop among STAT3, EGFR, and NF-κB that mediates primary resistance to STAT3 blockade and suggest strategies for therapeutic intervention.

Key Points

1. Inhibition of STAT3 activated EGFR through BTC.
2. Inhibition of STAT3 cooperated with neutralizing antibody against BTC to induce apoptosis in glioblastoma cells.
3. Blockade of STAT3 and EGFR inhibited growth of orthotopic PDX tumors, leading to improved survival in vivo.

Importance of the Study

Glioblastoma is the most common primary brain tumor, and among the most lethal of cancers. Dysregulated STAT3 signaling is found in a majority of tumors. Although activation of STAT3 correlates with malignancy and poor prognosis in glioblastoma, tumors show primary resistance to STAT3 inhibition. Here, we clarify the basis for this resistance, demonstrating that blockade of STAT3 triggers a rapid adaptive response. We trace this adaptive response to increased secretion of the EGFR ligand BTC. BTC activates the EGFR:NF-κB signaling axis in an autocrine manner, thereby attenuating the antitumor activity of STAT3 blockade. Neutralizing antibody to BTC rendered glioma cells sensitive to STAT3 inhibition. Combined inhibition of both STAT3 and EGFR disabled this autocrine activation loop, representing a rational approach for patients with *EGFR*-amplified GBM.

The infiltrating gliomas show a spectrum of histopathologies, with high-grade glioblastoma (GBM) tumors both the most common and the most lethal. A broad disconnect exists between scientific insights into the biology of GBM and the translation of these basic observations into improved outcomes for patients. Activation of signal transducer and activator of transcription 3 (STAT3) promotes GBM growth and survival by modulating transcription of genes regulating stemness, angiogenesis, and the tumor microenvironment.[1] Perhaps not surprisingly, activation of STAT3 also correlates with poor outcome in patients.[2–4] These observations suggest STAT3 blockade as a therapeutic strategy; however, GBM cells demonstrate primary resistance to STAT3 inhibition.[5,6]

Here we clarify the basis of this resistance. Blockade of STAT3 leads to activation of epidermal growth factor receptor (EGFR) and subsequent activation of nuclear factor-kappaB (NF-κB), also a major mediator of resistance in GBM.[1,7] Activation of EGFR in the context of STAT3 inhibition occurs due to synthesis and secretion of the EGFR ligand betacellulin (BTC). BTC-driven activation of EGFR subsequently drives phosphorylation of NF-κB. As an approach to interfere with this feedback, we demonstrate that STAT3 inhibition cooperates with a neutralizing antibody to BTC, inducing apoptosis in GBM. Our findings identify a new interaction between STAT3 and EGFR, with implications for therapy.

Methods

Cell Lines, Reagents, Transfection, and Transduction

Human GBM cell lines LN229, U87, SF767, and U251 obtained from the Brain Tumor Research Center at UCSF, were grown in Dulbecco's modified Eagle's medium with 10% fetal bovine serum as described.[8] Patient-derived xenograft (PDX) glioma specimens GBM8 and GBM43 obtained from Dr C. David James, were grown in neurobasal complete medium supplemented with B27, N2, 20 ng/mL epidermal growth factor (EGF) and 20 ng/mL fibroblast growth factor (FGF). All cells have been tested and authenticated. Mycoplasma status is checked monthly in the lab using the human embryonic kidney (HEK)–blue detection kit (InvivoGen). Control small interfering (si)RNA, STAT3, and NF-kB p65 siRNA were purchased from Dharmacon. Cells were transfected with siRNA using Lipofectamine 2000 (Invitrogen) as directed by the manufacturer. Stattic, STAT3 short hairpin (sh)RNA, and control shRNA were purchased from Sigma-Aldrich. To generate retrovirus to transduce EGFR, the packaging cell line HEK293T was co-transfected with pWLZ-hygro-EGFR, gag/pol, and VSVg plasmids using Effectene-transfection reagent (Qiagen). High-titer virus collected at 48 h was used to transduce cells as described.[9] Transduced cells were selected as pools with hygromycin (500 μg/mL) for 2 weeks. EGF (Roche), cycloheximide, Stattic, Bay11-7085 (Sigma), osimertinib (Selleck Chemicals), granulocyte-macrophage colony-stimulating factor (GM-CSF), interleukin (IL)-6, IL-8, and tumor necrosis factor alpha (TNF-α) (Cell Signaling) were purchased from commercial vendors. Erlotinib tablets (Genentech) were ground to powder and dissolved in aqueous HCl, and the aqueous phase was extracted with ethyl acetate.

Cell Proliferation Assays and Apoptosis Detection

For proliferation, 5×10^4 cells were seeded in 12-well plates and treated as indicated for 3 days. Proliferation was determined by water-soluble tetrazolium salt (WST-1) assay (Roche) and analyzed by spectrophotometry. Each sample was assayed in triplicate and absorbance at 450 nm was read on a plate reader after 40 min. Apoptosis was detected by western blotting for cleaved poly(ADP-ribose) polymerase (PARP) and flow cytometry for annexin V.

Human Phospho-Receptor Tyrosine Kinase Array

Activation/phosphorylation of receptor tyrosine kinases (RTKs) was analyzed using human phospho-RTK array kits (R&D Systems #ARY001B and Cell Signaling #7982). Cells were treated as indicated for 24 h. A total of 500 μg of protein, determined by bicinchoninic acid (BCA) assay, was used for each array, and the assay was performed according to the manufacturer's protocols.

Human Cytokine Antibody Array

To investigate the secretion/expression of cytokines, we used a human cytokine antibody array kit (Abcam

#ab133996). Cells were treated as indicated for 24 h. An equal amount of culture supernatant or a total of 200 μg of protein from cell lysates, determined by the BCA assay, was used for each array and the assay was performed according to the manufacturer's protocols.

Subcellular Fractionation

For multi-compartmental fractionation of cells, we used a subcellular protein fractionation kit (Thermo Scientific Pierce) according to the manufacturer's instructions.

EGFR Ligand Antibody Array

To study the secretion/expression of EGFR ligands, we used a customized human cytokine antibody array kit (RayBiotech). Cells were transfected with control siRNA or STAT3 siRNA for 48 h, and culture supernatant was collected from an equal amount of cells. The supernatant was filtered through 0.45 μM filters. Cells were lysed using ice-cold cell lysis buffer (50 mM Tris-HCl, 150 mM NaCl, 1 mM EDTA, 1% Triton X-100) with protease inhibitor cocktail. Protein concentration was measured by the BCA assay. The antibody array was performed according to the manufacturer's instructions.

Betacellulin Enzyme-Linked Immunosorbent Assay

To measure the secretion/expression of BTC, cells were transfected with control siRNA or STAT3 siRNA for 48 h, and culture supernatant or cell lysate from an equal amount of cells was used for enzyme-linked immunosorbent assay (ELISA) according to the manufacturer's instructions (R&D Systems).

Quantitative Real-Time PCR

Cells were transfected with control siRNA or STAT3 siRNA. After 48 h, RNA was extracted using the Quick-RNA MiniPrep kit according to the manufacturer's instructions (Zymo Research). Complementary DNA was produced using the iScript cDNA synthesis kit (Biorad). Quantitative real-time (qRT)-PCR was performed using the SYBR FAST ABI Prism qPCR kit (KAPA Biosystems) on an AB7900HT real-time PCR machine (Applied Biosystems). The primers for BTC are: 5′-3′ CACAATCAAAGCGGAAAGGC; 5′-3′ TCTCACACCTTGCTCCAATG. The primers for glyceraldehyde 3-phosphate dehydrogenase (GAPDH) are: 5′-3′ AATCCCATCACCATCTTCCA; 5′-3′ TGGACTCCACGACGTACTCA.

EGFR Ligand Expression in Mouse and GBM Patient Tumors

Gene expression data from STAT3 knockout mice and control mice were downloaded from Gene Expression Omnibus (GEO) datasets with the accession number GDS3106 (https://www.ncbi.nlm.nih.gov/gds). Expression levels of the 7 EGFR ligands from 528 GBM patient samples were downloaded from http://gliovis.bioinfo.cnio.es/ (dataset: TCGA-GBM, platform HG-U133A). Correlation between EGFR ligands and STAT3 expression levels was analyzed using the online tool at http://gliovis.bioinfo.cnio.es/ (dataset: TCGA-GBM, platform HG-U133A).

Western Blotting

Membranes were blotted with p-EGFRY^{1173} (Novus Biologicals), EGFR, extracellular signal-regulated kinase 2 (ERK2) (Santa Cruz Biotechnology), p-AKT^{S473}, AKT, p-ERK$^{T202/Y204}$, p-STAT3^{Y705}, STAT3, p-IKK-α/β$^{S176/180}$, IKKβ, p-NF-kB p65^{S536}, NF-kB p65, lamin B1, cleaved PARP (Cell Signaling), GAPDH, β-tubulin (Upstate Biotechnology), and BTC (R&D Systems). Bound antibodies were detected with horseradish peroxidase–linked anti-mouse or anti-rabbit immunoglobulin G (Calbiochem), followed by electrochemiluminescence (Amersham).

In Vitro Luciferase Assay and Bioluminescence Imaging

Mice were injected i.p. with 64 mg/kg of D-luciferin (sodium salt; Gold Biotechnology) dissolved in sterile saline. Tumor bioluminescence was determined 20 min after D-luciferin injection using the IVIS Lumina System (Caliper Life Science) and Living Image software, as the sum of photon counts per second in regions of interest defined by a lower threshold value of 25% of peak pixel intensity. Imaging was performed every 4 days after tumor implantation until the last day on which all mice in compared groups were alive.

In Vivo Studies

All animal experiments were conducted using protocols approved by UCSF's Institutional Animal Use and Care Committee. For orthotopic injections and treatment studies, mice (4 to 6 wk old) were anesthetized using ketamine and xylazine. GBM43 cells (1×10^5) expressing firefly luciferase were injected intracranially (Hamilton syringe) at 2 mm anterior and 1.5 mm lateral of the right hemisphere relative to bregma, at a depth of 3 mm. Whole-brain bioluminescence was measured for each mouse every 4 days. When bioluminescence reached 10^5 photons/s, mice were sorted into 4 groups of equal bioluminescence signal in the vehicle and osimertinib group or in the STAT3 shRNA and STAT3 shRNA plus osimertinib group (6 mice per group) and therapy initiated. Mice were treated by oral gavage of vehicle (0.5% hydroxypropyl methylcellulose [HPMC], 0.1% Tween 80 in H_2O, daily) or osimertinib (25 mg/kg, daily) for 18 days. Mice were monitored daily and euthanized when exhibiting neurological deficits or 15% reduction from initial body weight.

Immunohistochemical Analyses

Immunohistochemical (IHC) sections were prepared by the UCSF Brain Tumor Research Center Tissue Core. After resection, mouse brains (3 mice per group) were fixed for

48 h in 4% paraformaldehyde in phosphate buffered saline. Brains were then paraffin embedded, and sectioned (5 μm) for hematoxylin and eosin staining and IHC analyses. For IHC, slides were deparaffinized, and antigen retrieval was performed using a pressure cooker. The Vectastain ABC reagent (Vector laboratories) was used for signal detection. The cleaved caspase-3 and Ki67 antibodies were purchased from Cell Signaling and used at a concentration of 1:100. Images were taken using a Nikon *Eclipse* microscope.

Statistical Analyses

Survival analysis was performed using the GraphPad program; significance was determined by the log-rank (Mantel–Cox) test. For all analyses, a 2-tailed paired Student's *t*-test was applied.

Results

Inhibition of STAT3 Activates NF-κB and Increases Production of NF-κB–Dependent Cytokines

We and others have previously demonstrated that glioblastoma cells show primary resistance to STAT3 blockade.[5,6] To understand contributors to this resistance, we identified cytokines, the abundance of which was significantly altered in response to inhibition of STAT3. For LN229:*EGFR* cells in response to treatment with the STAT3 activation and dimerization inhibitor Stattic,[10] levels of IL-8, GM-CSF, and IL-6 protein were increased significantly in cellular supernatants, with levels of GM-CSF and IL-6 also increased in lysates (Fig. 1A and Supplementary Fig. 1). We also observed similar increase of at least one of those cytokines in U87:*EGFR* cells and GBM8 cells (Fig. 1A). Because GM-CSF, IL-6, and IL-8 are downstream target genes of the NF-κB signaling pathway,[11] we asked whether inhibition of STAT3 activated NF-κB signaling. Both inhibition and knockdown of STAT3 led to increased phosphorylation of the RelA subunit of NF-κB (Fig. 1B, 1C). The NF-κB (inhibitor of kappa B kinase [IKK]) inhibitor Bay 11-7085[12] blocked subsequent secretion of GM-CSF, IL-6, and IL-8, and abrogated the ability of these cells to activate IKK in response to STAT3 inhibition (Fig. 1D, 1E). While none of these cytokines affected the phosphorylation of EGFR, IL-6 stimulation, as expected, led to phosphorylation of STAT3 (Fig. 1F). These data demonstrate that blockade of STAT3 induced phosphorylation of NF-κB in glioblastoma cells. Activated NF-κB drove increased expression of GM-CSF, IL-6, and IL-8, with IL-6 reinforcing activation of STAT3.

Inhibition or Knockdown of STAT3 Activates EGFR without Affecting Other RTKs

Since NF-κB is downstream of EGFR,[13,14] we next analyzed phosphorylation of EGFR following inhibition or siRNA knockdown of STAT3. As expected, Stattic reduced the abundance of p-STAT3^{Y705} (Fig. 2A). Interestingly, levels of p-EGFR^{Y1173} increased after Stattic treatment in multiple GBM cell lines, independently of mutational status of phosphatase and tensin homologue (*PTEN*) (Fig. 2A and Supplementary Fig. 2A–C). To rule out off-target effects of Stattic, we knocked down STAT3 using siRNA. Knockdown of STAT3 similarly induced p-EGFR^{Y1173} (Fig. 2B). Across 5 of 6 lines tested, the increased abundance of p-EGFR was generally similar comparing siRNA and Stattic treatment (Supplementary Fig. 2C). In GBM43 cells, Stattic induced higher levels of p-EGFR compared with shRNA treatment, perhaps related to the different mechanisms through which Stattic and siRNA block STAT3 signaling (inhibition of STAT3 activation and nuclear entry vs decreased abundance of total STAT3 protein). Overexpression of EGFR was not required for this effect, as activation of EGFR in response to STAT3 inhibition was also observed in cells without EGFR overexpression (Supplementary Fig. 2D). Next we asked whether RTKs in addition to EGFR were activated in response to inhibition of STAT3. In LN229 cells overexpressing EGFR, among 49 human RTKs assayed in a human phospho-RTK array, only the abundance of p-EGFR increased following STAT3 inhibition (Fig. 2C, D and Supplementary Fig. 2E–J). In the LN229 parental cells without EGFR overexpression, dot plot results showed that EGFR was also the only RTK activated, again indicating that overexpression of EGFR is not required for this effect (Supplementary Fig. 2K–M). To test if Stattic treatment changed the rate of turnover for EGFR, we measured EGFR half-life using the protein synthesis inhibitor cycloheximide. In response to blockade of STAT3, the half-life of EGFR protein was unchanged by addition of cycloheximide. These results demonstrate that pharmacologic inhibition and genetic knockdown of STAT3 activate EGFR signaling and that inhibition of STAT3 drives EGFR phosphorylation independently of receptor stability (Fig. 2E, F).

A Feedback Loop Links STAT3, EGFR, and NF-κB Signaling in Glioblastoma

To test whether activation of EGFR in response to STAT3 inhibition actually induced phosphorylation of NF-κB, we treated LN229:*EGFR* cells with Stattic and analyzed signaling changes over time. Phosphorylation of EGFR started at 3 h and continued through 24 h, correlating with sustained phosphorylation of NF-κB (Fig. 3A). Treatment of cells with an EGFR inhibitor (erlotinib) abrogated the EGFR-driven activation of NF-κB and STAT3 (Fig. 3B).

To further address how STAT3 converges on EGFR and NF-κB signaling, we separately analyzed signaling changes in membrane, cytoplasmic, and nuclear fractions in LN229:*EGFR* cells. Total EGFR, NF-κB, and STAT3 proteins were detected in membrane, cytoplasmic, and nuclear extracts. Both p-EGFR and p-NF-κB were detected mainly in cytoplasmic extracts, while p-STAT3 was detected mainly in nuclear extracts. Stattic treatment resulted in increased phosphorylation of EGFR and NF-κB in both cytoplasmic and nuclear extracts, and decreased phosphorylation of STAT3 in the nucleus (Fig. 3C). The relative intensity of p-EGFR, p-NF-κB, and p-STAT3 in each fraction at baseline was set to 100% after normalization (β-tubulin for membrane fractions, GAPDH for cytoplasmic fractions, lamin

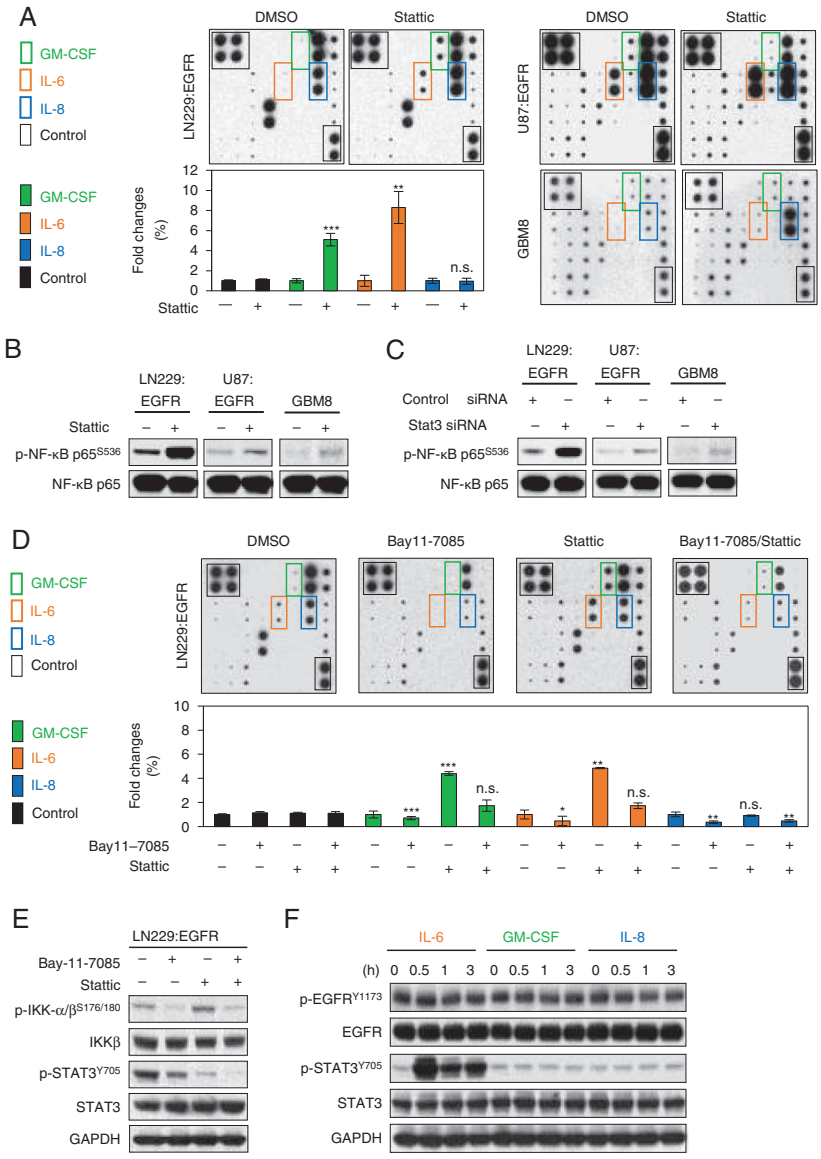

Fig. 1 Inhibition of STAT3 increases production of NF-κB-dependent cytokines. (A) LN229:*EGFR*, U87:*EGFR*, and GBM8 cells were treated with DMSO or 3 μM Stattic for 24 h. Supernatant were prepared and used to assess 23 human cytokines with a human cytokine antibody array kit. GM-CSF, IL-6, IL-8, and control are boxed and labeled. Intensity of GM-CSF, IL6, and IL8 from LN229:*EGFR* cells was quantified by densitometry using a Silver Fast Scanner and ImageJ software. Data shown represent mean ± SD of quadruplicate measurements from two independent experiments. Fold changes were normalized to DMSO-treated control. ***$P < 0.001$, vehicle versus Stattic (GM-CSF); **$P = 0.0011$, vehicle versus Stattic (IL-6); no significant, vehicle versus Stattic (IL-8) by two-tailed Student's t-test. (B) LN229:*EGFR*, U87:*EGFR*, and GBM8 cells were treated with 3 μM Stattic for 24 h, harvested, lysed, and analyzed by western blotting with indicated antibodies. For the expression levels of EGFR or GAPDH in each cell line, see Fig. 2A. (C) LN229:*EGFR*, U87:*EGFR*, and GBM8 cells were transfected with control siRNA or STAT3 siRNA for 48 h, harvested, lysed, and analyzed by western blot with indicated antibodies. For the expression levels of EGFR or GAPDH in each cell line, see Fig. 2B. (D) LN229:*EGFR* cells were treated with DMSO, 3 μM Stattic, 3 μM Bay11-7085, or Stattic plus Bay11-7085 for 24 h. These profiles obtained by incubating the array membranes with supernatant are shown. GM-CSF, IL-6, IL-8, and control are boxed and labeled. Intensity of GM-CSF, IL6, and IL8 was quantified by densitometry using a Silver Fast Scanner and ImageJ software. Data shown represent mean ± SD of quadruplicate measurements from 2 independent experiments. Fold changes were normalized to DMSO-treated control. For intensity of GM-CSF, ***$P = 0.0003$, vehicle versus Bay11-7085; ***$P = 0.0002$, vehicle versus Stattic; no significant, vehicle versus Bay-11-7085 plus Stattic. For intensity of IL6, *$P = 0.0238$, vehicle versus Bay11-7085; **$P = 0.0012$, vehicle versus Stattic; no significant, vehicle versus Bay-11-7085 plus Stattic. For intensity of IL8, **$P = 0.0038$, vehicle versus Bay11-7085; no significant, vehicle versus Stattic; **$P = 0.0018$, vehicle vs Bay-11-7085 plus Stattic by two-tailed Student's *t*-test. (E) LN229:*EGFR* cells treated with 3 μM Stattic, 3 μM Bay11-7085, or 3 μM Stattic plus 3 μM Bay11-7085 for 24 h, harvested, lysed, and analyzed by western blot with indicated antibodies. (F) LN229:*EGFR* cells were treated with IL-6 (10 ng/mL), GM-CSF (1 ng/mL), or IL-8 (100 ng/mL) for indicated time (0.5–3 h), harvested, lysed, and analyzed by western blot with antibodies indicated. See also Supplementary Fig. 1.

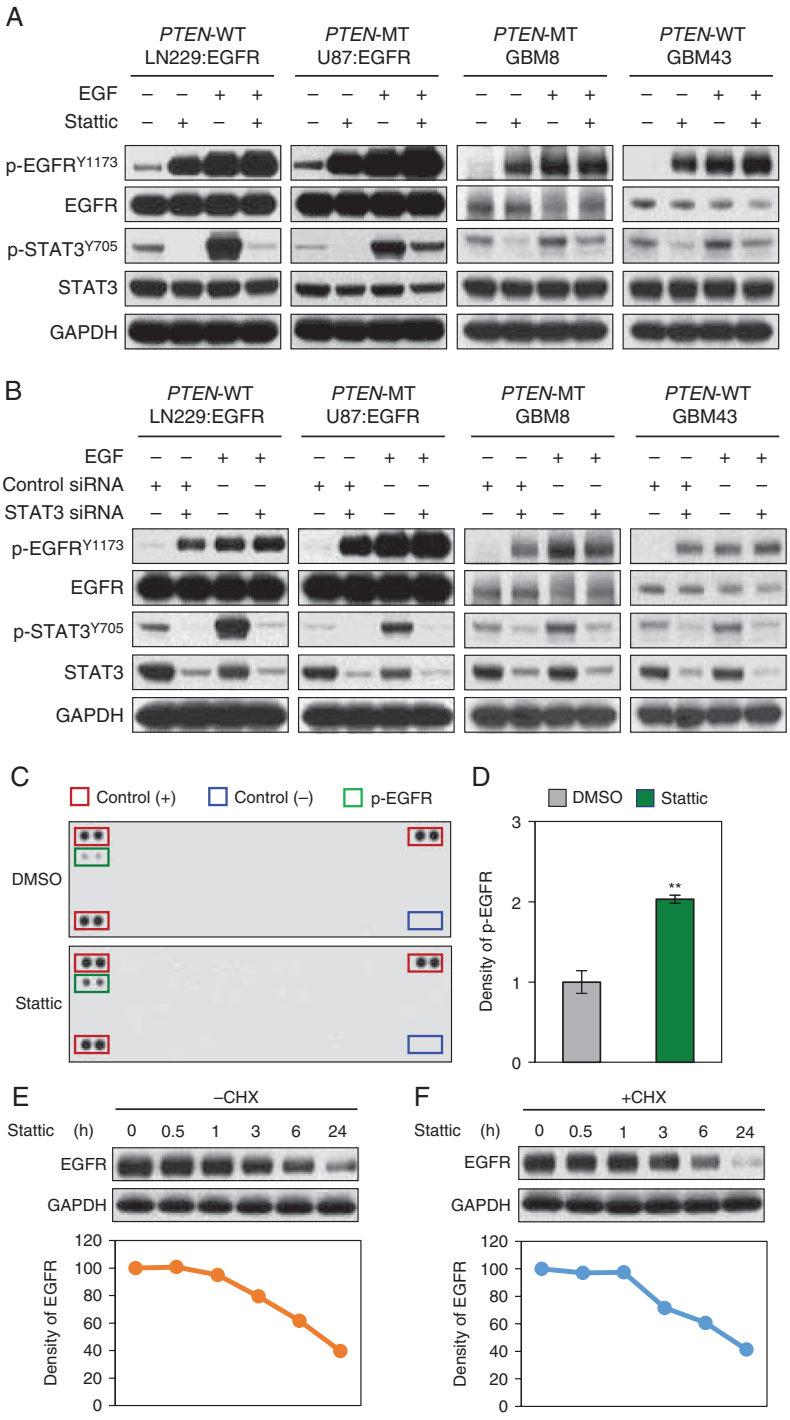

Fig. 2 Inhibition or knockdown of STAT3 activates EGFR without affecting other RTKs. (A) Cell lines shown were treated with 3 μM Stattic for 24 h. EGF (50 ng/mL) was added 15 min before harvest, and lysates were analyzed by western blot with indicated antibodies. (B) Cells as in (A) were transfected with control siRNA or STAT3 siRNA for 48 h. EGF (50 ng/mL) was added 15 min before harvest, and lysates analyzed. (C) LN229:*EGFR* cells were treated with DMSO or 3 μM Stattic for 24 h. Cell lysates were prepared and used to assess tyrosine phosphorylation of 49 human RTKs. Boxes indicate manufacturer's positive and negative controls, and location of p-EGFR. (D) The intensity of p-EGFR was quantified by densitometry using a Silver Fast Scanner and ImageJ software. Data shown represent mean ± standard deviation of quadruplicate measurements from 2 independent experiments. Fold changes were normalized to DMSO-treated control. $^{**}P = 0.0010$ vehicle vs Stattic (two-tailed Student's *t*-test). (E, F) LN229:*EGFR* cells were treated with 3 μM Stattic in the presence or absence of cycloheximide (CHX, 50 μg/mL) for indicated time (0.5–24 h), harvested, lysed, and analyzed by western blot with antibodies indicated. Band intensities for EGFR were quantified by densitometry using a Silver Fast Scanner and ImageJ software; after normalization to GAPDH (bottom panel). See also Supplementary Fig. 2.

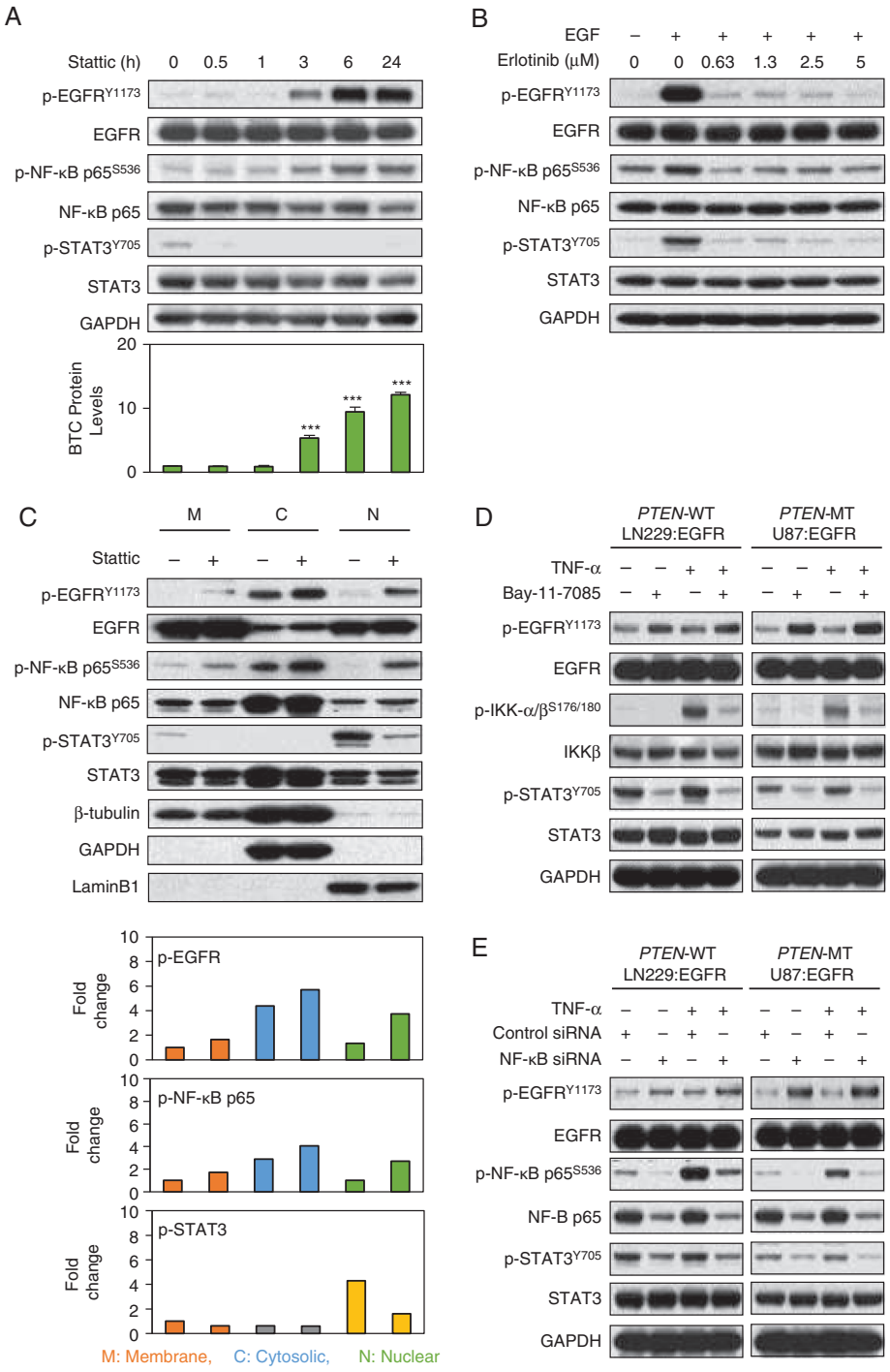

Fig. 3 A negative feedback loop links STAT3 to EGFR-NF-κB signaling. (A) LN229:*EGFR* cells were treated with 3 μM Stattic for indicated times, harvested, lysed, and analyzed by western blot with indicated antibodies (top panel). LN-229:EGFR cells were treated as in (A). Supernatants were collected, and levels of BTC were measured using ELISA. Data shown represent mean ± SD of triplicate measurements. ***$P < 0.001$ (two-tailed Student's *t*-test, bottom panel). (B) LN229:*EGFR* cells were treated with erlotinib at doses indicated (0–5 μM) for 24 h. EGF (50 ng/mL) was added to cells 15 min before harvest, and lysates analyzed by western blot. (C) LN229:*EGFR* cells were treated with 3 μM Stattic for 24 h, harvested and subjected to subcellular fractionation to obtain membrane (M), cytoplasmic (C), and nuclear (N) extracts, and analyzed by western blot. Efficiency of subcellular fractionation is indicated by a membrane/cytoplasmic marker protein β-tubulin, a cytoplasmic marker protein GAPDH, and a nuclear marker protein lamin B1 (top panel). Band intensities of p-EGFR, p-NF-κB p65, and p-STAT3 from (top panel) were quantified by densitometry. Band intensities were normalized to β-tubulin for membrane, GAPDH for cytoplasmic fraction, and lamin B1 for nuclear fractions. (D) LN229:*EGFR* and U87:*EGFR* cells were treated with 3 μM Bay11-7085 for 24 h. TNF-α (20 ng/mL) was added to cells 30 min before harvest, and lysates analyzed by western blot. (E) LN229:*EGFR* and U87:*EGFR* Cells were transfected with control siRNA or NF-κB p65 siRNA for 48 h. TNF-α (20 ng/mL) was added to cells 30 min before harvest, and lysates were analyzed by western blot. See also Supplementary Fig. 3.

B1 for nuclear fractions). In response to Stattic treatment for 24 h, the relative abundance of p-EGFR and p-NF-κB in membrane fractions increased to 164% and 172%, respectively, and p-STAT3 decreased to 62%. The relative abundance of p-EGFR and p-NF-κB in cytoplasmic fractions increased to 130% and 140%, respectively, and p-STAT3 remained essentially unchanged (98%). The relative abundance of p-EGFR and p-NF-κB in nuclear fractions increased to 278% and 267%, respectively, and p-STAT3 decreased to 37%. These data suggest that Stattic treatment led to increased phosphorylation of EGFR and NF-κB primarily in the nucleus (Fig. 3C).

We next tested whether inhibitors of NF-κB could block STAT3 and thereby increase the abundance of p-EGFR. LN229:*EGFR*, SF767:*EGFR*, U87:*EGFR*, and U373:*EGFR* cells were treated with Bay 11-7085 (an inhibitor of IKK) in the absence or presence of TNF-α to induce the NF-κB pathway. In response to Bay 11-7085, cells showed decreased levels of p-IKK-α/β$^{S176/180}$ and p-STAT3, and increased levels of p-EGFR. Activation of NF-κB in response to TNF-α led to increased abundance of p-IKK-α/β and p-STAT3. This TNF-α–induced activation of NF-κB and STAT3 was blocked by Bay 11-7085 (Fig. 3D and Supplementary Fig. 3). Similar results were obtained using siRNA against NF-κB p65 (Fig. 3E). Results in Fig. 3 describe a feedback loop in GBM linking STAT3 inhibition to activation of EGFR and downstream NF-κB signaling, and NF-κB in turn activating STAT3.

Inhibition of STAT3 Activates the EGFR Ligand BTC

The most common mechanism for EGFR activation is ligand-mediated receptor phosphorylation. EGFR ligands activate EGFR within seconds.[15,16] We therefore asked whether inhibition of STAT3 led to increased production of EGFR ligands. We treated cells with control or STAT3 siRNA and collected conditioned media. Using this media to treat cells in the absence of siRNA transfection, we observed increased phosphorylation of EGFR at 5 minutes, continuing through 60 minutes, and then declining after 2 h (Fig. 4A). These data indicate that one or more EGFR ligands EGF, transforming growth factor alpha (TGF-α), heparin-binding EGF-like growth factor (HB-EGF), amphiregulin (AREG), BTC, epiregulin (EREG), and epigen (EPGN)[17]) are driving activation. To address which EGFR ligands are expressed in GBM, we analyzed mRNA expression of EGF ligands using the database of The Cancer Genome Atlas (TCGA) from 528 GBM patients (HG-U133A, http://cancergenome.nih.gov/). All ligands except for EPGN were expressed (Supplementary Fig. 4A). To evaluate correlations, we analyzed mRNA expression of STAT3 and the 6 EGFR ligands expressed in human GBM in TCGA. A significant negative correlation was found between expression of STAT3 and BTC or EREG (Supplementary Fig. 4B). Levels of STAT3 did not correlate with levels of EGF, TGFA, or AREG. Levels of STAT3 correlated positively with levels of HB-EGF (Supplementary Fig. 4B). Moreover, among the 6 EGFR ligands expressed in GBM, the mRNA level of BTC was uniquely and significantly higher in epithelial cells of STAT3 null mice compared with wild-type mice (GEO: GDS3106)[18] (Supplementary Fig. 4C).

To test whether inhibition of STAT3 led to increased production of BTC, EREG, or other EGFR ligands, we generated an array spotted with antisera against each of 6 human EGFR ligands expressed in GBM. The abundance of BTC increased most significantly in both cellular supernatants and lysates following STAT3 siRNA treatment, with little to no change observed among other EGF ligands (Fig. 4B). By ELISA the abundance of BTC in conditioned media increased significantly in response to STAT3 siRNA, compared with the control (Fig. 4C). Increased levels of BTC protein were observed in the conditioned medium after 3 h of Stattic treatment, consistent with the time frame for EGFR activation (Fig. 3A). BTC protein levels at 24 h Stattic treatment were higher than at 6 h; however, levels of p-EGFRY^{1173} level were comparable, likely due to saturation of receptor activation (Fig. 3A). To test whether knockdown of STAT3 increased transcription of BTC, we performed qRT-PCR. In response to STAT3 siRNA treatment, levels of BTC mRNA were increased (Fig. 4D). We next asked whether the increased production of BTC led to activation of EGFR in response to STAT3 blockade. Eliminating BTC from the conditioned media using a BTC neutralizing antibody blocked STAT3 siRNA-induced EGFR phosphorylation (Fig. 4E). To generalize this result, and to validate disease relevance, we analyzed primary human GBM specimens obtained by surgical resection before therapy. Expression of STAT3 and BTC proteins in these specimens generally showed an inverse correlation (Fig. 4F, Supplementary Fig. 5). Together, these data indicated that knockdown of STAT3 stimulates synthesis and secretion of BTC, activating EGFR through an autocrine mechanism.

Dual Blockade of STAT3 and BTC Induces Apoptosis in GBM Cells

We next asked whether blockade of BTC could decrease activation of EGFR and NF-κB in response to inhibition of STAT3 and whether dual blockade of STAT3 and BTC could cooperate in GBM. As expected, inhibition of STAT3 with Stattic, but not dimethyl sulfoxide (DMSO) led to increased abundance of p-NF-κB. This increase was blocked by a BTC neutralizing antibody. Combining Stattic with neutralizing antibody to BTC led to significant increases in apoptosis and decreases in proliferation compared with either monotherapy in LN229:*EGFR*, U87:*EGFR*, and GBM43 cells (Fig. 5A and Supplementary Fig. 6A). Similar results were observed with STAT3 siRNA treatment (Fig. 5B and Supplementary Fig. 6B). These results suggested that activation of EGFR in response to STAT3 blockade is mediated by BTC and that combined blockade of both STAT3 and of BTC cooperate to inhibit growth and induce apoptosis of GBM.

Dual Blockade of STAT3 and EGFR Inhibits Tumor Growth In Vivo

BTC neutralizing antibodies do not cross the blood–brain barrier. However, EGFR, the effector molecule of

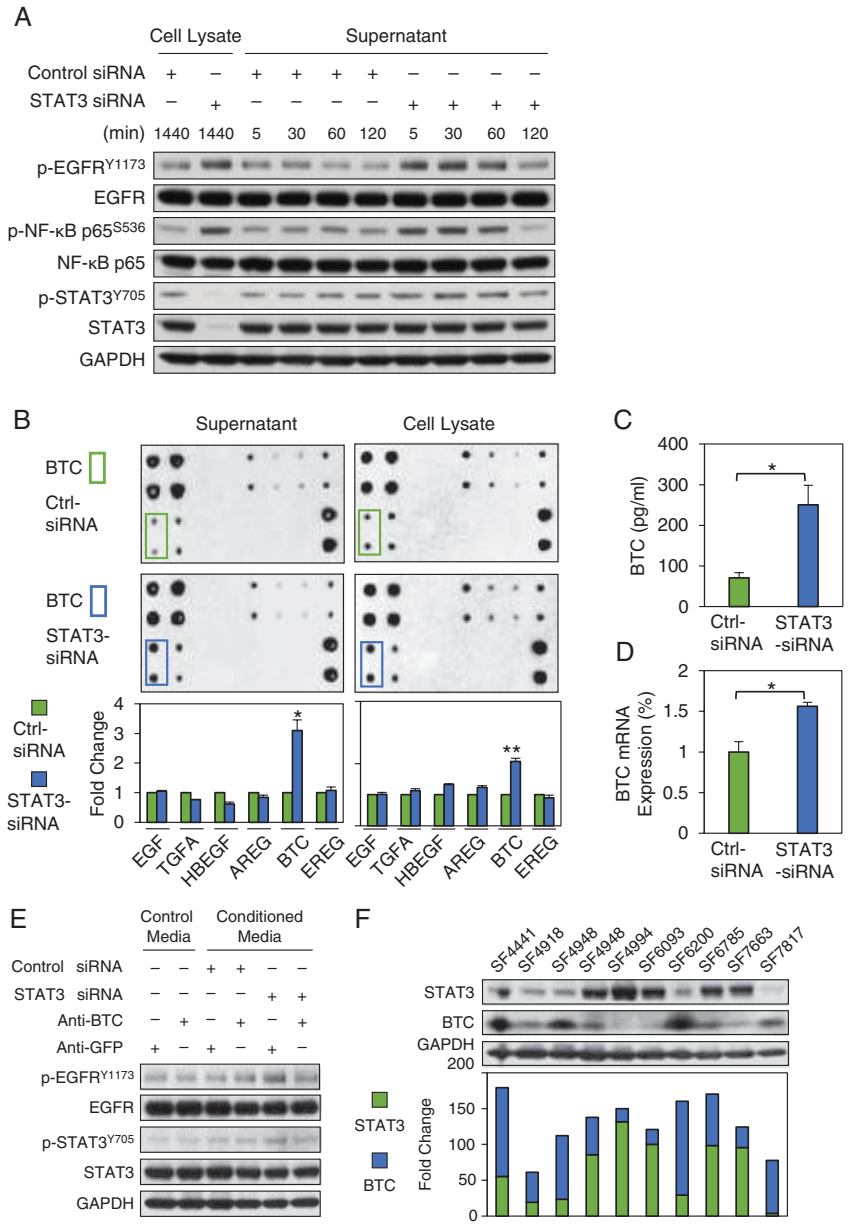

Fig. 4 Expression of BTC and STAT3 show and inverse correlation. (A) LN229:*EGFR* cells were transfected with control siRNA or STAT3 siRNA for 48 h, harvested, lysed, and analyzed by western blot with antibodies indicated. Supernatants were collected and used to treat LN229:*EGFR* cells for indicated times. Cells were harvested, and lysates analyzed by western blot with antibodies indicated. (B) LN229:*EGFR* cells were transfected with control siRNA or STAT3 siRNA. After 48 h, supernatants and cell lysates were used to assess expression of indicated human EGFR ligands in an antibody array. Boxes indicate location of BTC. Intensity of EGF ligands was quantified by densitometry using a Silver Fast Scanner and ImageJ software. Fold changes were normalized to the difference in signal between positive and negative controls. Data shown represent mean ± SD of quadruplicate measurements from 2 independent experiments. $^{**}P = 0.0058$, control siRNA versus STAT3 siRNA in supernatants; $^{**}P = 0.006$, control siRNA versus STAT3 siRNA in cell lysate (two-tailed Student's *t*-test). (C) LN-229:EGFR cells were treated as in (B). Supernatants were collected, and levels of BTC were measured using a ELISA. Data shown represent mean ± SD of triplicate measurements. $^{*}P = 0.0221$, control siRNA versus STAT3 siRNA (two-tailed Student's *t*-test). (D) LN229:*EGFR* cells were treated as in (B). Total RNA was used for qRT-PCR analysis of BTC. Data shown represent mean ± SD. Fold increases are relative to control siRNA and normalized to GAPDH of triplicate measurements. $^{*}P = 0.014$, control siRNA versus STAT3 siRNA (two-tailed Student's *t*-test).(E) LN229:*EGFR* cells were treated as in B. DMEM with 10% FBS (used as negative control) or conditioned media were incubated with 10 μg/mL BTC neutralizing antibody or with 10 μg/mL GFP antibody for 2 h, and were used to treat LN229:*EGFR* cells for 30 min. The cells were harvested, lysed, and the lysates analyzed by western blot with indicated antibodies. (F) Human glioblastoma samples from the Brain Tumor Research Center at UCSF were lysed and analyzed by western blot with the antisera indicated (top panel). The intensity of STAT3 and BTC were normalized to GAPDH and quantified by densitometry using a Silver Fast Scanner and ImageJ software (bottom panel).

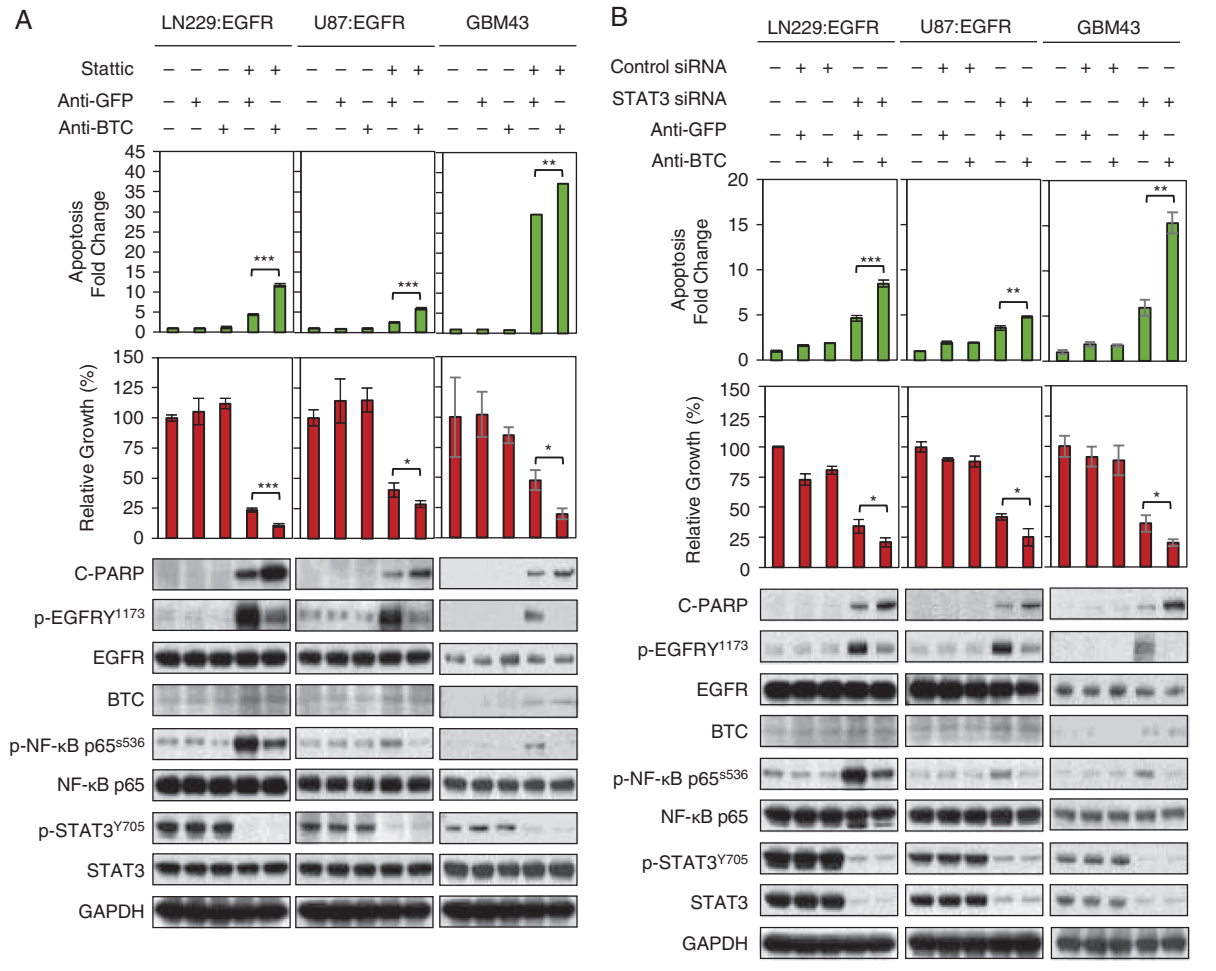

Fig. 5 Combinatory inhibition of STAT3 and BTC induces apoptosis in glioblastoma cells. (A) LN229:*EGFR*, U87:*EGFR*, and GBM43 cells were treated with 10 μg/mL control GFP antibody, 10 μg/mL BTC neutralizing antibody, 3 μM Stattic plus 10 μg/mL GFP antibody, or 3 μM Stattic plus 10 μg/mL BTC neutralizing antibody for 2 days for apoptosis and biochemical analyses; and 3 days for proliferation. Apoptosis was measured by flow cytometric with annexin V-FITC conjugates, and proliferation by WST-1 assay. Data shown represent mean ± SD of triplicate measurements. ***P = 0.0001, 3 μM Stattic plus green fluorescent protein (GFP) neutralizing antibody versus 3 μM Stattic plus BTC neutralizing antibody in LN229:*EGFR* cells; ***P = 0.0001, 3 μM Stattic plus GFP neutralizing antibody versus 3 μM Stattic plus BTC neutralizing antibody in U87:*EGFR* cells; **P = 0.0011, 3 μM Stattic plus GFP neutralizing antibody versus 3 μM Stattic plus BTC neutralizing antibody in U87:*EGFR* cells (two-tailed Student's *t*-test, top panel). Proliferation was measured by WST-1 assay. Data shown represent mean ± SD of triplicate measurements (middle panel). ***P = 0.0007, 3 μM Stattic plus GFP neutralizing antibody versus 3 μM Stattic plus BTC neutralizing antibody in LN229:*EGFR* cells; *P = 0.0013, 3 μM Stattic plus GFP neutralizing antibody versus 3 μM Stattic plus BTC neutralizing antibody in U87:*EGFR* cells (two-tailed Student's *t*-test). Cells were treated as in (A) for 48 h, Cells were treated as in (A) for 48 h, harvested, lysed, and analyzed by western blot with antibodies indicated (bottom panel). (B) LN229:*EGFR*, U87:*EGFR*, and GBM43 cells were treated with 10 μg/mL GFP neutralizing antibody, 10 μg/mL BTC neutralizing antibody, control siRNA plus 10 μg/mL GFP neutralizing antibody or STAT3 siRNA plus 10 μg/mL BTC neutralizing antibody for 3 days (top panel). Proliferation was measured by WST-1 assay. Data shown represent mean ± SD of triplicate measurements (top panel). *P = 0.0272, control siRNA plus GFP neutralizing antibody versus STAT3 siRNA plus BTC neutralizing antibody in LN229:*EGFR* cells; *P = 0.0204, control siRNA plus GFP neutralizing antibody versus STAT3 siRNA plus BTC neutralizing antibody in U87:*EGFR* cells; **P = 0.0075, 3 μM Stattic plus GFP neutralizing antibody versus 3 μM Stattic plus BTC neutralizing antibody in GBM43 cells (two-tailed Student's *t*-test, top panel). Cells were treated as in (A) for 48 h, apoptosis was measured by flow cytometric with annexin V-FITC conjugates (middle panel). Data shown represent mean ± SD of triplicate measurements (middle panel). ***P = 0.0002, control siRNA plus GFP neutralizing antibody versus STAT3 siRNA plus BTC neutralizing antibody in LN229:*EGFR* cells; **P = 0.0017, control siRNA plus GFP neutralizing antibody versus STAT3 siRNA plus BTC neutralizing antibody in U87:*EGFR* cells (two-tailed Student's *t*-test). Cells were treated as in A for 48 h, harvested, lysed, and analyzed by western blot with antibodies indicated (bottom panel). See also Supplementary Fig. 5.

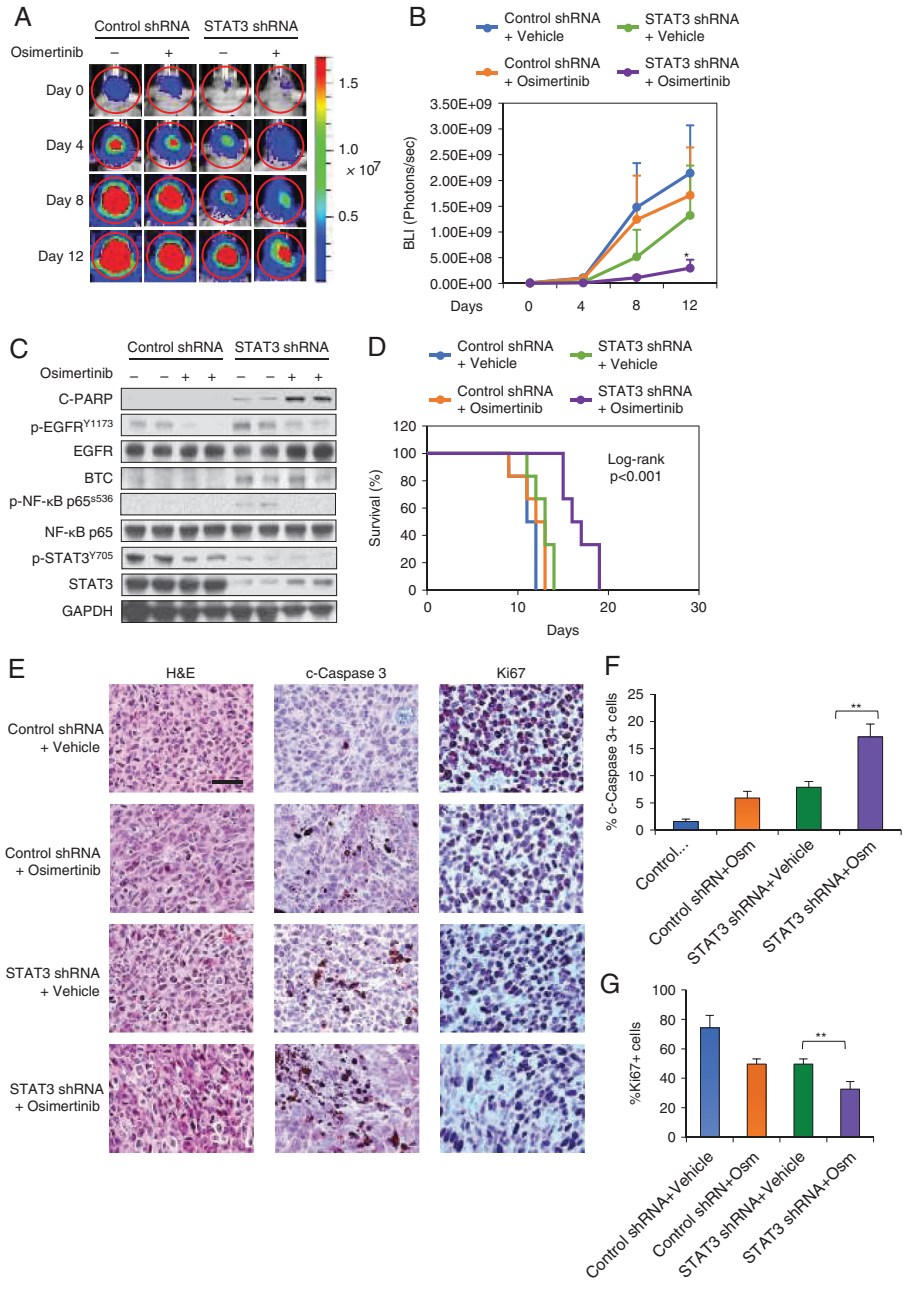

Fig. 6 Knockdown of STAT3 cooperates with inhibition of EGFR in an orthotopic PDX GBM model. GBM43 cells (1×10^5) expressing firefly luciferase were injected intracranially in BALB/$c^{nu/nu}$ mice. After tumor establishment, mice were sorted into four groups and treated by oral gavage of vehicle (daily), or osimertinib (25 mg/kg, daily). (A) Bioluminescence imaging of tumor-bearing mice was obtained at days shown (day 0 was start of treatment), using identical imaging conditions. (B) Dynamic measurements of bioluminescence intensity (BLI) in treated tumors over time. Regions of interest (ROIs) from displayed images were revealed on the tumor sites and quantified as maximum photons/s/cm^2 squared/steradian. Data shown are means of photon flux ± SD from n = 6 mice. Not significant: vehicle versus osimertinib. Significant: $^*P = 0.0377$, vehicle versus STAT3 shRNA; $^*P = 0.0296$, vehicle versus STAT3 shRNA plus osimertinib (two-tailed Student's *t*-test on day 8). Not significant, vehicle versus osimertinib; $^*P = 0.0409$, vehicle versus STAT3 shRNA plus osimertinib (two-tailed Student's *t*-test on day 12). (C) Animals were euthanized when showing signs of illness, as per IACUC protocol. Two animals from each group treated as in (A) were treated by oral gavage of vehicle or osimertinib (25 mg /kg) 2 h prior to being euthanized. Tumors were harvested, lysed, and analyzed by western blot with antibodies indicated. (D) Survival curves of BALB/$c^{nu/nu}$ mice injected intracranially with GBM43 cells. Three days after tumor implantation, mice were treated as in (A). Not significant: vehicle versus osimertinib. Significant: $^*P = 0.00103$, vehicle versus STAT3 shRNA, $^{**}P = 0.00103$, vehicle versus STAT3 shRNA plus osimertinib; $^*P = 0.0249$, osimertinib versus STAT3 shRNA; $^{**}P = 0.00105$, osimertinib versus STAT3 shRNA plus osimertinib; $^{***}P < 0.001$, STAT3 shRNA versus STAT3 shRNA plus osimertinib (log-rank analysis; $n = 6$ mice per group). (E) Hematoxylin and eosin and IHC staining of cleaved caspase-3 and Ki67. (F and G) Quantification of cleaved caspase-3 ($P = 0.0019$) and Ki67 ($P = 0.0051$) positive cells. Scale bar: 50 μM.

BTC-EGFR, can be inhibited using the third-generation EGFR inhibitor osimertinib, which was shown to cross the blood–brain barrier well.[19] In addition, osimertinib is clinically available and can be used to treat patients.[19] To test the effect of dual blockade of BTC-mediated EGFR activation and STAT3, we stably expressed control shRNA or STAT3 shRNA in luciferase-expressing GBM43 cells and injected the resulting cells into the forebrains of nude mice. Mice were treated by oral gavage of vehicle (0.5% HPMC, 0.1% Tween 80 in H_2O, daily) or osimertinib (25 mg/kg, daily) for 18 days. While no survival benefit was observed in response to monotherapy using either shRNA against STAT3 or osimertinib (Fig. 6), combined blockade of EGFR and STAT3 led to a significant survival benefit, as well as decreased tumor growth measured by luciferase imaging (Fig. 6A, 6B, 6D). Dual blockade of EGFR and STAT3 led to increased levels of BTC in vivo, also associated with increased levels of cleaved PARP and cleaved caspase-3, and decreased levels of Ki67 in tumors (Fig. 6C, E, F, G). These data indicate that blocking EGFR can help to overcome resistance to STAT3 therapeutics in GBM.

To address whether this feedback loop extended to other EGFR-driven cancers, we analyzed PC9 cells. In this lung adenocarcinoma line, blockade of EGFR with osimertinib also led to inhibition of STAT3 (Supplementary Fig. 7) and induction of BTC mRNA and protein (Supplementary Fig. 7). Together, these data indicated that knockdown of STAT3 stimulates synthesis and secretion of BTC, activating EGFR through an autocrine mechanism.

Discussion

EGFR amplification and overexpression are hallmarks of GBM. EGFR signals to downstream targets, including STAT3 and NF-κB, pathways linked to therapy resistance and poor outcome in patients,[2,3,20,21] reviewed by Gray et al[1]. The resulting activation of STAT3 promotes glioma stem cells, tumor-intrinsic progression, and immune invasion.[1] Given its central role in progression and resistance, STAT3 would appear to be an ideal target for therapy. Perhaps surprisingly, however, our experiments, inhibiting STAT3 using siRNA or the tool compound Stattic, demonstrated that GBM cells showed primary resistance to STAT3 blockade.[5]

EGFR signaling is regulated by a large number of ligands, each of which can activate EGFR and downstream signaling pathways. We traced primary resistance in STAT3-driven GBM cell lines to increased production of BTC. In GBM cells, we showed that EGFR activated NF-κB. NF-κB in turn activated STAT3, and STAT3 blocked transcription of BTC. We extended relevance beyond GBM as well, studying therapy-resistant non–small cell lung cancer cells, which we showed express BTC as a mechanism of acquired resistance to EGFR tyrosine kinase inhibitors (Supplementary Fig. 7).

BTC was initially identified in the conditioned media of cells derived from mouse tumors, and its overexpression was observed in human cancers.[22,23] BTC is a potent mitogen, regulating cell proliferation and stemness.[23,24] Although BTC can activate all possible heterodimeric combinations of the ERBB receptor family,[24,25] our results showed that activation of ERBB kinases in response to STAT3 inhibition or knockdown was specific to EGFR. EGFR is likely the predominant ERBB receptor in GBM. If EGFR molecules are more abundant than other ERBBs, this may result in BTC inducing relatively low level activation ERBB receptor of family members.

The prominent role of STAT3 in cancers has been firmly established,[26] and a number of STAT3 inhibitors are in development.[27–30] Completed clinical trials have not yet shown promise in solid tumors.[31,32] Our finding that STAT3 inhibition leads to secretion of BTC and subsequent activation of EGFR and NF-κB provides new insights into mechanisms of resistance. Our preclinical data that combined blockade of STAT3 and EGFR led to improved survival in mice with orthotopic PDX tumors in vivo suggest a rationale for combinatorial therapy.

Supplementary Material

Supplementary data are available at *Neuro-Oncology* online.

Keywords

glioblastoma | STAT3 | BTC | NF-κB | feedback loop

Funding

This work was supported by National Institutes of Health (R01NS091620, R01NS089868, R01CA148699, U01CA217864, P30CA82103, U54CA163155 and P50AA017072 to W.A.W, R01CA221969 to Q.F., W.A.W., and K.M.S., T32CA108462 to Z.A.); American Brain Tumor Association Basic Research Fellowship in honor of Juliana Schafer and Team Hope to Z.A., R01CA231300, U54CA224081, R01CA204302, R01CA211052, R01CA169338 and U01CA217882 to T.G.B., Children's Tumor, Marcus Precision Medicine Innovation Award, Ross K. MacNeill, and the Samuel Waxman Cancer Research Foundation to W.A.W.

Conflict of interest statement. W.A.W is a co-founder of StemSynergy Therapeutics.

Authorship statement. Conception, design, and development of methodology: Q.F., Z.A., A.B., K.M.S., T.G.B., and W.A.W. Data acquisition, analysis, and interpretation: Q.F., Z.A., R.A.W., X.L., E.L., M.K.M., and F.H. Writing of manuscript: Q.F., Z.A., and W.A.W. Study supervision: W.A.W.

References

1. Gray GK, McFarland BC, Nozell SE, Benveniste EN. NF-κB and STAT3 in glioblastoma: therapeutic targets coming of age. *Expert Rev Neurother.* 2014;14(11):1293–1306.
2. Lin GS, Chen YP, Lin ZX, Wang XF, Zheng ZQ, Chen L. STAT3 serine 727 phosphorylation influences clinical outcome in glioblastoma. *Int J Clin Exp Pathol.* 2014;7(6):3141–3149.
3. Lin GS, Yang LJ, Wang XF, et al. STAT3 Tyr705 phosphorylation affects clinical outcome in patients with newly diagnosed supratentorial glioblastoma. *Med Oncol.* 2014;31(4):924.
4. Masliantsev K, Pinel B, Balbous A, et al. Impact of STAT3 phosphorylation in glioblastoma stem cells radiosensitization and patient outcome. *Oncotarget.* 2018;9(3):3968–3979.
5. Fan QW, Cheng CK, Gustafson WC, et al. EGFR phosphorylates tumor-derived EGFRvIII driving STAT3/5 and progression in glioblastoma. *Cancer Cell.* 2013;24(4):438–449.
6. Miyata H, Ashizawa T, Iizuka A, et al. Combination of a STAT3 inhibitor and an mTOR inhibitor against a temozolomide-resistant glioblastoma cell line. *Cancer Genomics Proteomics.* 2017;14(1):83–91.
7. Puliyappadamba VT, Hatanpaa KJ, Chakraborty S, Habib AA. The role of NF-κB in the pathogenesis of glioma. *Mol Cell Oncol.* 2014;1(3):e963478.
8. Fan QW, Cheng C, Hackett C, et al. Akt and autophagy cooperate to promote survival of drug-resistant glioma. *Science Signaling.* 2010; 3(147):ra81.
9. Fan QW, Knight ZA, Goldenberg DD, et al. A dual PI3 kinase/mTOR inhibitor reveals emergent efficacy in glioma. *Cancer Cell.* 2006;9(5):341–349.
10. Schust J, Sperl B, Hollis A, Mayer TU, Berg T. Stattic: a small-molecule inhibitor of STAT3 activation and dimerization. *Chem Biol.* 2006;13(11):1235–1242.
11. Brasier AR. The nuclear factor-kappaB-interleukin-6 signalling pathway mediating vascular inflammation. *Cardiovasc Res.* 2010;86(2):211–218.
12. Mori N, Yamada Y, Ikeda S, et al. Bay 11-7082 inhibits transcription factor NF-kappaB and induces apoptosis of HTLV-I-infected T-cell lines and primary adult T-cell leukemia cells. *Blood.* 2002;100(5):1828–1834.
13. Jiang T, Grabiner B, Zhu Y, et al. CARMA3 is crucial for EGFR-Induced activation of NF-κB and tumor progression. *Cancer Res.* 2011;71(6):2183–2192.
14. Biswas DK, Cruz AP, Gansberger E, Pardee AB. Epidermal growth factor-induced nuclear factor kappa B activation: amajor pathway of cell-cycle progression in estrogen-receptor negative breast cancer cells. *Proc Natl Acad Sci U S A.* 2000;97(15):8542–8547.
15. Madshus IH, Stang E. Internalization and intracellular sorting of the EGF receptor: a model for understanding the mechanisms of receptor trafficking. *J Cell Sci.* 2009;122(Pt 19):3433–3439.
16. Reddy RJ, Gajadhar AS, Swenson EJ, Rothenberg DA, Curran TG, White FM. Early signaling dynamics of the epidermal growth factor receptor. *Proc Natl Acad Sci U S A.* 2016;113(11):3114–3119.
17. An Z, Aksoy O, Zheng T, Fan QW, Weiss WA. Epidermal growth factor receptor and EGFRvIII in glioblastoma: signaling pathways and targeted therapies. *Oncogene.* 2018;37(12):1561–1575.
18. Xu Y, Ikegami M, Wang Y, Matsuzaki Y, Whitsett JA. Gene expression and biological processes influenced by deletion of Stat3 in pulmonary type II epithelial cells. *BMC Genomics.* 2007;8:455.
19. Wu YL, Ahn MJ, Garassino MC, et al. CNS efficacy of osimertinib in patients with T790M-positive advanced non-small-cell lung cancer: data from a randomized phase III trial (AURA3). *J Clin Oncol.* 2018;36(26):2702–2709.
20. Shinojima N, Tada K, Shiraishi S, et al. Prognostic value of epidermal growth factor receptor in patients with glioblastoma multiforme. *Cancer Res.* 2003;63(20):6962–6970.
21. Heimberger AB, Hlatky R, Suki D, et al. Prognostic effect of epidermal growth factor receptor and EGFRvIII in glioblastoma multiforme patients. *Clin Cancer Res.* 2005;11(4):1462–1466.
22. Yokoyama M, Funatomi H, Kobrin M, et al. Betacellulin, a member of the epidermal growth-factor family, is overexpressed in human pancreatic-cancer. *Int J Oncol.* 1995;7(4):825–829.
23. Shing Y, Christofori G, Hanahan D, et al. Betacellulin: a mitogen from pancreatic beta cell tumors. *Science.* 1993;259(5101):1604–1607.
24. Dahlhoff M, Wolf E, Schneider MR. The ABC of BTC: structural properties and biological roles of betacellulin. *Semin Cell Dev Biol.* 2014;28:42–48.
25. Riese DJ 2nd, Bermingham Y, van Raaij TM, Buckley S, Plowman GD, Stern DF. Betacellulin activates the epidermal growth factor receptor and erbB-4, and induces cellular response patterns distinct from those stimulated by epidermal growth factor or neuregulin-beta. *Oncogene.* 1996;12(2):345–353.
26. Johnson DE, O'Keefe RA, Grandis JR. Targeting the IL-6/JAK/STAT3 signalling axis in cancer. *Nat Rev Clin Oncol.* 2018;15(4):234–248.
27. Sen M, Thomas SM, Kim S, et al. First-in-human trial of a STAT3 decoy oligonucleotide in head and neck tumors: implications for cancer therapy. *Cancer Discov.* 2012;2(8):694–705.
28. Bendell JC, Hong DS, Burris HA 3rd, et al. Phase 1, open-label, dose-escalation, and pharmacokinetic study of STAT3 inhibitor OPB-31121 in subjects with advanced solid tumors. *Cancer Chemother Pharmacol.* 2014;74(1):125–130.
29. Jung KH, Yoo W, Stevenson HL, et al. Multifunctional effects of a small-molecule STAT3 inhibitor on NASH and hepatocellular carcinoma in mice. *Clin Cancer Res.* 2017;23(18):5537–5546.
30. Huynh J, Etemadi N, Hollande F, Ernst M, Buchert M. The JAK/STAT3 axis: acomprehensive drug target for solid malignancies. *Semin Cancer Biol.* 2017;45:13–22.
31. Oh DY, Lee SH, Han SW, et al. Phase I study of OPB-31121, an oral STAT3 inhibitor, in patients with advanced solid tumors. *Cancer Res Treat.* 2015;47(4):607–615.
32. Wong ALA, Hirpara JL, Pervaiz S, Eu JQ, Sethi G, Goh BC. Do STAT3 inhibitors have potential in the future for cancer therapy? *Expert Opin Investig Drugs.* 2017;26(8):883–887.